Dalton Transactions

ROYAL SOCIETY OF CHEMISTRY

PAPER

View Article Online
View Journal

Cite this: DOI: 10.1039/d4dt01863j

β-Cyclodextrin and cucurbit[7]uril as protective encapsulation agents of the CO-releasing molecule [CpMo(CO)$_3$Me]†

Rodrigo P. Monteiro, [a] Isabel B. Calhau, [a] Ana C. Gomes, [a] André D. Lopes, [b] José P. Da Silva,[b] Isabel S. Gonçalves *[a] and Martyn Pillinger *[a]

The CO releasing ability of the complex [CpMo(CO)$_3$Me] (**1**) (Cp = η^5-C_5H_5) has been assessed using a deoxymyoglobin-carbonmonoxymyoglobin assay. In the dark, CO release was shown to be promoted by the reducing agent sodium dithionite in a concentration-dependent manner. At lower dithionite concentrations, where dithionite-induced CO release was minimised, irradiation at 365 nm with a low-power UV lamp resulted in a strongly enhanced release of CO (half-life ($t_{1/2}$) = 6.3 min), thus establishing complex **1** as a photochemically activated CO-releasing molecule. To modify the CO release behaviour of the tricarbonyl complex, the possibility of obtaining inclusion complexes between **1** and β-cyclodextrin (βCD) or cucurbit[7]uril (CB7) by liquid–liquid interfacial precipitation (**1**@βCD(IP)), liquid antisolvent precipitation (**1**@CB7), and mechanochemical ball-milling (**1**@βCD(BM)) was evaluated. All these methods led to the isolation of a true inclusion compound (albeit mixed with nonincluded **1** for **1**@βCD(BM)), as evidenced by powder X-ray diffraction (PXRD), thermogravimetric analysis (TGA), FT-IR and FT-Raman spectroscopies, and $^{13}C\{^1H\}$ magic angle spinning (MAS) NMR. PXRD showed that **1**@βCD(IP) was microcrystalline with a channel-type crystal packing structure. High resolution mass spectrometry studies revealed the formation of aqueous phase 1 : 1 complexes between **1** and CB7. For **1**@βCD(IP) and **1**@CB7, the protective effects of the hosts led to a decrease in the CO release rates with respect to nonincluded **1**. βCD had the strongest effect, with a *ca.* 10-fold increase in $t_{1/4}$ for dithionite-induced CO release, and a *ca.* 2-fold increase in $t_{1/2}$ for photoinduced CO release.

Received 27th June 2024,
Accepted 5th November 2024

DOI: 10.1039/d4dt01863j

rsc.li/dalton

Introduction

Carbon monoxide (CO) is a colourless, odourless, and tasteless gas produced from the incomplete combustion of carbonaceous fuels and biomass. The discovery of CO is generally credited to Joseph Priestley who, in 1772, obtained the gas by heating iron oxide (Fe_3O_4) with charcoal.[1] It was not until 1801 when the chemical composition was resolved by William Cruickshank, who named the molecule 'gaseous oxide of carbon'.[2] Cruickshank's discovery was the springboard for research focused solely on CO. Although most studies during the late 1700s and 1800s were concerned with the toxicological profile of CO and its mechanism of action as a toxic substance, it is remarkable that medicinal uses were investigated, *e.g.*, as a local and general anaesthetic, analgesic, and for the treatment of ailments such as infectious diseases and respiratory illness.[3] Despite several advances during the 20th century that led to the recognition of CO as an endogenously produced signalling molecule,[4] the image of CO as a deadly gas persisted and it was only after the turn of the century that CO started to be widely explored as a therapeutic agent owing to its beneficial physiological effects in processes like vasorelaxation, anti-inflammation, anti-proliferation and anti-apoptosis.[5]

Following numerous successes with inhaled CO in preclinical animal studies,[6] several hospital-based clinical trials were initiated to examine safety and efficacy in humans.[7,8] However, the implementation of CO gas therapy in a hospital setting raises technical and safety-related issues, and this method of CO delivery suffers from other disadvantages such as lack of targetability.[9] These limitations led to the search for small-molecule drugs, termed CO-releasing molecules (CORMs), that could be used in pharmaceutical formulations

[a]*CICECO – Aveiro Institute of Materials, Department of Chemistry, University of Aveiro, Campus Universitário de Santiago, 3810-193 Aveiro, Portugal. E-mail: igoncalves@ua.pt, mpillinger@ua.pt*

[b]*Centre of Marine Sciences (CCMAR/CIMAR LA), and Department of Chemistry and Pharmacy, FCT, University of the Algarve, 8005-039 Faro, Portugal*

†Electronic supplementary information (ESI) available: ^{1}H NMR spectrum of **1**, ESI figures for gas-phase ESI-HRMS studies, ATR FT-IR and UV-vis spectra for (photo)stability studies of **1**, CO release profiles for **1** and the inclusion compounds using 0.4% sodium dithionite, CO release profiles for **1** to check for dithionite dependence. See DOI: https://doi.org/10.1039/d4dt01863j

for the solid or liquid dosage of CO.[9–12] The pioneers in this field were Motterlini and co-workers who realised that transition metal carbonyl complexes could be ideal vehicles to carry and deliver CO to biological targets owing to their well-known capacity to release CO upon the action of chemical (*e.g.*, hydrolysis) or photochemical triggers.[13–15] It is notable that as long ago as 1891 McKendrick and Snodgrass suggested that nickel tetracarbonyl, the first metal carbonyl compound, could be used for the oral delivery of CO, exerting an antipyretic action.[16,17] However, $Ni(CO)_4$ is highly toxic and therefore unsuitable as a therapeutic agent. Over the last two decades, Motterlini and co-workers, followed by many other groups, have developed a huge library of CORMs based on biologically acceptable metals such as Fe, Mn, Co, Mo and Ru, the first four of which have essential functions in living systems.

Research on molybdenum complexes as potential metallopharmaceuticals[18] has been emboldened by the knowledge that, on the one hand, this element plays an essential role in human health,[19] and, on the other, Mo metabolites are expected to have low toxicity.[20] The interest in organomolybdenum drugs was sparked by the discovery by Köpf and Köpf-Maier that molybdenocene dichloride, Cp_2MoCl_2 (Cp = η^5-C_5H_5) exhibited cytotoxic activity against different cancer cell lines with lower toxicity than cisplatin.[21] A potentially advantageous feature of Cp_2MoCl_2 and its derivatives is the hydrolytic stability of the Cp ligands at physiological pH.[22–24] Besides bis(cyclopentadienyl) molybdenum complexes, mono (cyclopentadienyl) half-sandwich complexes have also been quite widely explored for various biological applications.[24] For example, the complex $[CpMo(NO)_2Cl]$ was found to be an effective nitrovasodilator *in vitro* and *in vivo* through the release of nitric oxide.[25] Regarding mono(cyclopentadienyl) molybdenum carbonyl complexes, these have been studied as labelling agents for biomolecules,[26] cytotoxic agents against human and nonhuman cancer cell lines,[27–31] and CORMs (Fig. 1).[32–34]

Most of the previous molybdenum carbonyl complexes that have been studied as CORMs (Fig. 1) were used in their discrete molecular form.[20,32–47] To improve the solubility and/or stability of CORMs in aqueous media, secure a sustained and controlled CO release, and mitigate potential toxicity associated with the metal decarbonylation fragments, conjugated CORM carrier or host–guest systems have been developed.[48–50] Mo-based CORM conjugates reported to date were obtained by the immobilisation of the isocyanoacetate complexes $[Mo(CO)_3(CNCR_2CO_2H)_3]$ (R = H, Me) in metal–organic frameworks (MOFs)[51,52] and a layered double hydroxide,[53] and $Mo(CO)_6$ in a MOF.[54] Although not studied specifically in the context of CO-based therapy, inclusion compounds of $[CpMo(CO)_3Cl]$ with β-cyclodextrin (CD) and permethylated βCD (TRIMEB) were previously described.[55,56] CDs are non-toxic cyclic oligomers of glucose that are firmly established as pharmaceutical adjuvants due to their ability to improve the aqueous solubility, physical chemical stability, and bioavailability of hydrophobic drug molecules.[57,58] Another family of macrocyclic drug delivery vehicles are cucurbit[*n*]urils (CB*n*), which are methylene-linked oligomers of glycoluril that have a symmetric 'barrel' shape with a hydrophobic cavity and two identical carbonyl-lined portals.[59] Harding and co-workers were the first to show that CB*n* could form host : guest complexes with potential organomolybdenum drugs, namely Cp_2MoCl_2.[60] We recently described inclusion complexes of CB7 and CB8 with $[CpMo(CO)_3Me]$ and their use in epoxidation catalysis.[61] It was since found that CO release rates from $[(\eta^5\text{-}C_5H_4CO_2CH_3)Mo(CO)_3Me]$, in aqueous media with or without photoactivation, could be modified by encapsulation of the complex in CB8.[62]

The present work set out to comprehensively evaluate organic cavitands as molecular containers for CORMs by comparing CDs and CBs as hosts for the complex $[CpMo(CO)_3Me]$. We chose this complex because, on the one hand, it is readily available, being easily prepared by literature methods, and, on the other, the portal diameters (5.4–6.0 Å) and cavity sizes (6.5–7.3 Å) of βCD and CB7 are ideally suited to the encapsulation of Cp-ligands with a diameter of *ca.* 5.7 Å. Equimolar CORM@(βCD/CB7) solid compounds were prepared by different methods, *i.e.*, co-grinding or coprecipitation from solution, and characterised by thermogravimetric analysis, powder X-ray diffraction, infrared spectroscopy and solid-state ^{13}C NMR spectroscopy. Host–guest complex formation in solution has been studied by mass spectrometry. Finally, the CO release behaviours of the compounds under simulated physiological conditions are compared.

Experimental

Starting materials and chemicals

All reagents and solvents were obtained from commercial sources and used as received. For synthesis: molybdenum hexacarbonyl (technical grade, Sigma-Aldrich), 2.4 M sodium cyclopentadienylide in THF (Sigma-Aldrich), methyl iodide (99%, Sigma-Aldrich), β-cyclodextrin (kindly donated by Laboratories La Rouquette, France, water content 10 mol mol^{-1}) and dichloromethane (99%, Riedel de Haën). For the Mb assays: Mb from equine skeletal muscle (95–100%, lyophilised powder), sodium dithionite (≥82%), phosphate buffered saline (PBS) tablet (to prepare 10 mM phosphate buffer), 4-(2-hydroxyethyl)piperazine-1-ethanesulfonic acid (HEPES; 99.5%) and carbon monoxide (99.9%) were obtained from Sigma-Aldrich, and Alphagaz Nitrogen type 1 (99.9%) was purchased from AirLiquide. Anhydrous solvents, namely dimethyl sulfoxide (99.9%, Merck), absolute ethanol (99.9%, Carlo Erba), diethyl ether (99%, Sigma-Aldrich), THF (≥99.9%, Sigma-Aldrich) and hexane (99%, Carlo Erba), were stored over 4 Å molecular sieves.

Methods

Powder X-ray diffraction (PXRD) data were collected at room temperature on a Malvern Panalytical Empyrean diffractometer equipped with a spinning flat sample holder and a PIXcel 1D detector set at 240 nm from the sample, in a Bragg–Brentano *para*-focusing optics configuration. Cu-K$\alpha_{1,2}$ X-radiation (λ_1 =

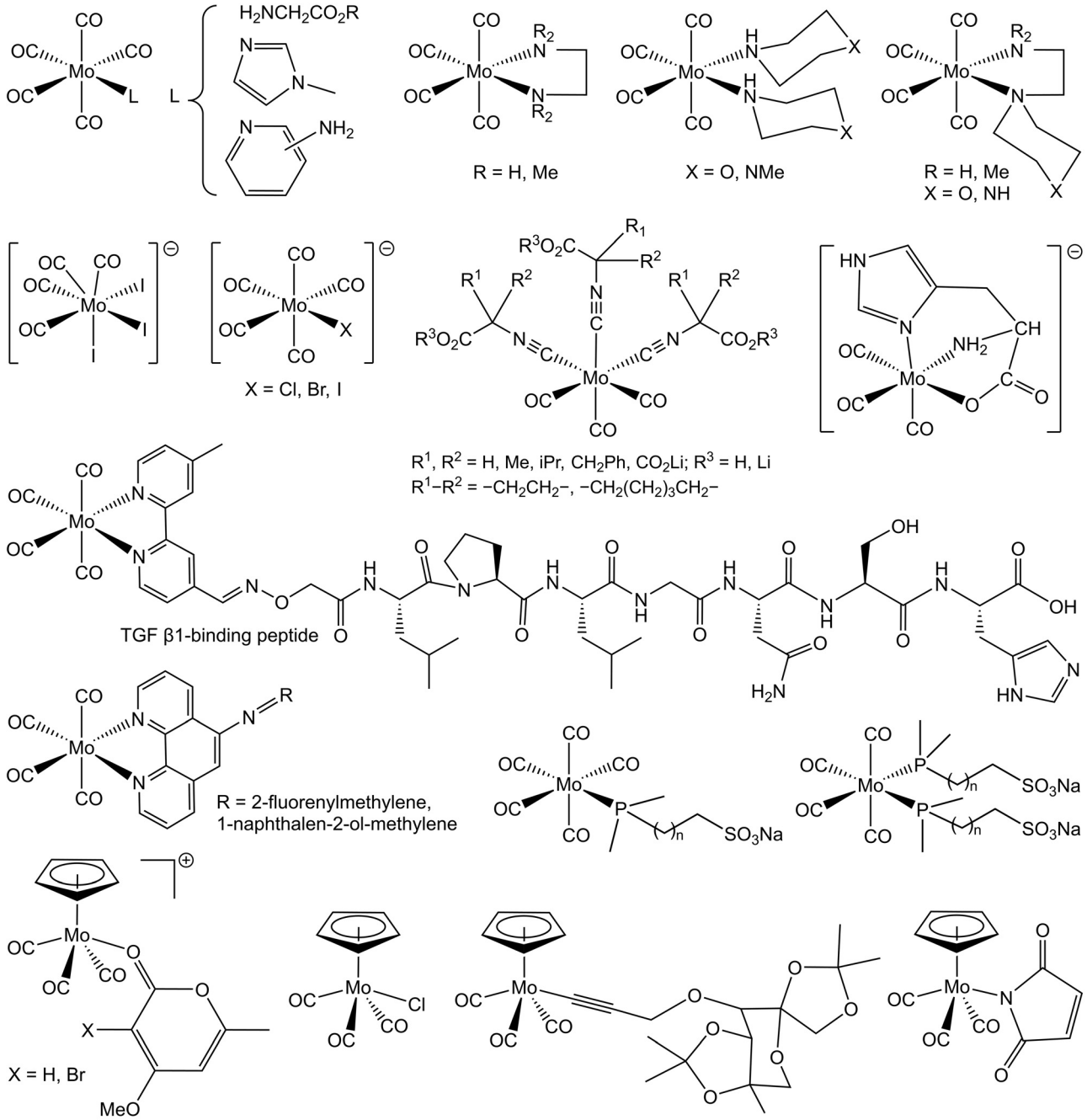

Fig. 1 Previous molybdenum carbonyl complexes that have been studied as CORMs.[20,32–47]

1.540598 Å, λ_2 = 1.544426 Å) filtered with nickel foil was used, with the X-ray tube operated at the voltage of 45 kV and the current of 40 mA. Samples were step-scanned from 3 to 70° (2θ) with step sizes of 0.02° and a counting time of 50 s per step. Thermogravimetric analysis (TGA) was performed under air using a HITACHI STA 300 system at a heating rate of 5 °C min^{-1}. Attenuated total reflectance (ATR) FT-IR spectra were measured on a Bruker Tensor 27 spectrometer equipped with a Specac Golden Gate Mk II ATR accessory having a diamond top plate and KRS-5 focusing lenses (resolution 4 cm^{-1}, 256 scans). FT-Raman spectra were recorded on a Bruker MultiRAM spectrometer equipped with a Nd:YAG laser with an excitation wavelength of 1064 nm (resolution 4 cm^{-1}, 1000 scans). ^{1}H and ^{13}C solution NMR spectra were obtained using a Bruker Avance III 300 MHz spectrometer. Chemical shifts are quoted in ppm from TMS. Solid-state $^{13}C\{^{1}H\}$ cross-polarisation (CP) magic-angle spinning (MAS) NMR spectra were recorded on a Bruker Avance III 400 spectrometer (9.4 T) at 100.62 MHz with 3.7 μs ^{1}H 90° pulses, 3500 ms contact time, spinning rate of 12 kHz, and 5 s recycle delays. For the Mb

assays, the UV-vis spectra were collected using a GBC 918 Cintral spectrophotometer. The UV-vis spectra for stability studies in solution were collected using a JASCO V-780 spectrophotometer. For stability studies and Mb assays performed with UV light (365 nm) exposure, a 15 W Velleman UV lamp was used as the light source (E = 2.5 mW cm^{-2}).

For separations by centrifugation, a Hettich Zentrifugen Rotofix 32A centrifuge was used, working at a speed of 6000 rpm. Samples were loaded into 25 mL Falcon tubes.

Synthesis and stability studies

[CpMo(CO)$_3$Me] (1). The method described by Wilkinson[63] and later by King[64] was followed in which a solution of sodium cyclopentadienylide (0.44 g, 5.0 mmol) in dry THF (2.5 mL) was added to a suspension of $Mo(CO)_6$ (1.0 g, 3.8 mmol) in dry THF (20 mL), under a nitrogen atmosphere. After refluxing the mixture overnight, the solvent was removed by evaporation under reduced pressure, and the resultant solid was washed with diethyl ether (2 × 10 mL). The solid was then dissolved in THF (40 mL) and methyl iodide (0.7 mL, 11.4 mmol) was added, and the mixture was stirred at rt for 4 h. After removing the solvent under reduced pressure, the product was extracted with hexane (5 × 20 mL). The extractions were combined, giving a yellow solution, and complex **1** was obtained as a yellow solid after evaporation of the solution to dryness under reduced pressure. Purification was performed by sublimation of the solid at 60 °C. Yield: 0.62 g, 63%. Elemental analyses and the ^{1}H NMR spectrum (Fig. S1†) were consistent with expected data. FT-IR (ATR, cm^{-1}): 3904 (w), 3115 (w), 2981 (w), 2903 (w), 2816 (w), 2003 (s, ν_{CO}), 1890 (s, ν_{CO}), 1461 (w), 1421 (m), 1354 (w), 1262 (w), 1159 (m), 1084 (w), 1061 (m), 1009 (m), 924 (w), 914 (w), 821 (s), 580 (m), 559 (s), 481 (s), 449 (s), 403 (w), 354 (m). FT-Raman (cm^{-1}): 3125 (m), 2986 (w), 2907 (w), 2817 (w), 2006 (m, ν_{CO}), 1904 (s, ν_{CO}), 1425 (w), 1356 (w), 1164 (w), 1110 (s), 1063 (w), 826 (w), 581 (w), 485 (w), 455 (m), 440 (m), 407 (w), 357 (m), 337 (m), 176 (m), 106 (vs). ^{13}C{^{1}H} CP MAS NMR: δ = 241.6 (CO), 229.5 (CO), 93.9 (Cp), −23.5 (Me).

Stability studies of 1. In the solid-state: 20 mg of **1** was placed on a watch glass and exposed to air and light for 28 days. During that period, a series of ATR FT-IR spectra were collected. In solution: a sealed quartz UV-vis cell (3500 μL) was charged under an atmosphere of nitrogen with a magnetic stirring bar and a 400 μM solution of **1** in DMSO or ethanol. The cell was then kept in the dark for 6 h at 37 °C, with constant magnetic stirring, interrupting the incubation period every hour to record an absorption spectrum between 190 and 900 nm, with a scan speed of 200 nm min^{-1} and a slit width of 2 nm. An additional stability study was performed in which a 400 μM degassed solution of **1** in DMSO was exposed to UV light (365 nm) over a period of 2 h, interrupting the incubation every 30 min to record an absorption spectrum.

CB7. A sample of CB7 with the verified composition $C_{42}H_{42}N_{28}O_{14}\cdot11H_2O\cdot0.1HCl\cdot0.5(CH_3COCH_3)$ was synthesised and characterised as described previously.[65] The characterisation results were in excellent agreement with the published data.

1@βCD(BM). A 7 mL Teflon grinding jar was loaded with three yttrium-doped zirconia milling balls with a diameter of 3 mm, followed by a mixture of **1** (0.06 g, 0.22 mmol) and βCD (0.29 g, 0.22 mmol). The jar was transferred to a TMAXCN Vertical Planetary Ball Mill machine (XQM Series), and the mixture was milled for 48 h at rt, with a speed of 600 rpm. A pale-yellow solid was recovered, denoted as **1**@βCD(BM). Yield: 0.24 g, 71% (based on **1**·βCD·7.3H_2O). TGA of **1**@βCD(BM) revealed a mass loss of 8.6% from rt up to 130 °C, and a residual mass of 10.4% at 650 °C (calcd for **1**·βCD·7.3H_2O: 8.6% H_2O, 9.4% MoO_3 residue). FT-IR (ATR, cm^{-1}): 3288 (m), 2927 (w), 2012 (m, ν_{CO}), 1923 (s, ν_{CO}), 1641 (w), 1424 (w), 1366 (w), 1332 (w), 1300 (w), 1242 (w), 1152 (m), 1079 (m), 1022 (s), 999 (s), 937 (m), 844 (w), 824 (w), 755 (w), 646 (w), 562 (m), 526 (w), 486 (m), 443 (w), 409 (w), 377 (w). FT-Raman (cm^{-1}): 3108 (w), 2936 (m), 2901 (s), 2017 (m, ν_{CO}), 1930 (m, ν_{CO}), 1459 (w), 1425 (w), 1383 (w), 1330 (w), 1266 (w), 1254 (w), 1132 (w), 1110 (m), 1087 (w), 1065 (w), 1046 (w), 1030 (w), 948 (w), 864 (w), 823 (w), 756 (w), 705 (w), 598 (w), 577 (w), 554 (w), 481 (m), 451 (m), 410 (w), 357 (w), 336 (w), 285 (w), 241 (w), 176 (w), 100 (s). ^{13}C{^{1}H} CP MAS NMR: δ = 239.8 (CO), 228.1 (CO), 103.7 (βCD, C1) 93.6 (Cp), 92.0 (Cp), 81.6 (βCD, C4), 72.9 (βCD, C2,3,5), 60.2 (βCD, C6), −20.9 (Me), −23.2 (Me).

1@βCD(IP). Following the previously described method for the synthesis of a [CpMo(CO)$_3$Cl]@βCD inclusion compound by liquid–liquid interfacial precipitation,[55] a solution of **1** (0.06 g, 0.22 mmol) in dichloromethane (2 mL) was added to a solution of βCD (0.29 g, 0.22 mmol) in water (10 mL) at 40 °C, and the resultant mixture was stirred for 2 h (850 rpm). During this period, a pale-yellow precipitate formed at the interface between the two solutions. The solid was recovered by filtration, washed with dichloromethane (2 mL), deionised water (10 mL), and finally vacuum-dried at rt for 2 h. Yield: 0.20 g, 59% (based on **1**·βCD·8H_2O). Prior to characterisation, the solid was stored over water in a sealed desiccator at ambient temperature for several days. TGA of **1**@βCD(IP) revealed a mass loss of 9.3% from rt up to 130 °C, and a residual mass of 10.4% at 650 °C (calcd for **1**·βCD·8H_2O: 9.4% H_2O, 9.4% MoO_3 residue). FT-IR (ATR, cm^{-1}): 3291 (m), 2926 (w), 2895 (w), 2013 (m, ν_{CO}), 1929 (s, ν_{CO}), 1642 (w), 1424 (w), 1367 (w), 1332 (w), 1259 (w), 1203 (w), 1154 (m), 1103 (w), 1080 (m), 1024 (s), 1002 (s), 938 (m), 863 (w), 824 (w), 793 (w), 756 (w), 702 (w), 647 (w), 573 (m), 527 (w), 484 (w), 446 (w), 411 (w), 366 (m). FT-Raman (cm^{-1}): 3108 (w), 3087 (w), 2941 (m), 2900 (s), 2019 (m, ν_{CO}), 1934 (m, ν_{CO}), 1459 (w), 1424 (w), 1384 (w), 1337 (w), 1264 (w), 1205 (w), 1134 (w), 1110 (m), 1089 (w), 1065 (w), 1037 (w), 1004 (w), 950 (w), 866 (w), 777 (w), 758 (w), 708 (w), 651 (w), 597 (w), 579 (w), 482 (m), 451 (w), 435 (w), 407 (w), 356 (w), 333 (w), 174 (w), 98 (vs). ^{13}C{^{1}H} CP MAS NMR: δ = 239.2 (CO), 226.4 (CO), 103.6 (βCD, C1), 92.2 (Cp), 82.3, 81.0 (βCD, C4), 72.8 (βCD, C2,3,5), 60.4 (βCD, C6), −22.6 (Me).

1@CB7. Following the recently described procedure,[61] CB7 (0.20 g, 0.14 mmol) was added to a solution of **1** (0.04 g, 0.14 mmol) in ethanol (0.5 mL). Deionised water (20 mL) was then added, and the resultant suspension was stirred for 24 h at rt. The mixture was then centrifuged for 15 min, with a

speed of 6000 rpm. The light-yellow solid, denoted as **1**@CB7, was isolated by decantation of the mother liquor, and vacuum-dried for 2 h at rt. Yield: 0.14 g, 65% (based on **1**·CB7·9H_2O). TGA of **1**@CB7 revealed a mass loss of 9.8% from rt up to 200 °C, and a residual mass of 9.2% at 650 °C (calcd for **1**·CB7·9H_2O: 10.2% H_2O, 9.1% MoO_3 residue). FT-IR (ATR, cm^{-1}): 3441 (w), 2998 (w), 2923 (w), 2016 (m, ν_{CO}), 1921 (m, ν_{CO}), 1717 (m), 1459 (m), 1417 (m), 1373 (m), 1316 (m), 1225 (m), 1182 (m), 1153 (w), 1028 (w), 964 (m), 860 (w), 823 (w), 797 (s), 735 (m), 666 (m), 626 (w), 564 (w), 498 (w), 439 (w), 393 (w), 357 (m). FT-Raman (cm^{-1}): 3104 (w), 2993 (w), 2939 (s), 2754 (w), 2636 (w), 2018 (m), 1927 (s), 1743 (m), 1495 (w), 1422 (s), 1382 (s), 1325 (w), 1283 (w), 1230 (w), 1202 (w), 1189 (w), 1137 (w), 1112 (m), 1044 (w), 1011 (w), 972 (w), 900 (m), 829 (s), 753 (m), 711 (w), 684 (w), 656 (w), 511 (w), 471 (w), 458 (w), 439 (s), 366 (m), 336 (m), 289 (m), 185 (m), 94 (s), 63 (w). $^{13}C\{^1H\}$ CP MAS NMR: 224.2 (Mo–CO), 156.1 (N(CO)N), 96.6 (Cp), 71.3 (CH), 52.9 (CH_2), −18.9 (Me).

HRMSn

High resolution mass spectrometry studies were performed using an Orbitrap Elite (Thermo Scientific, Bremen, Germany) mass spectrometer. The mass spectrometer is composed of a linear ion trap analyser with MS*n*, n = 2–10 capability, and a high field high resolution orbitrap. The system was operated using a heated ESI ion source (HESI-II). Data were acquired under positive polarity. The flow was 5 μL min^{-1}. The ESI and ion optics parameters were the following: heater temperature 40 °C; sheath gas flow 10 arbitrary units; capillary temperature 325 °C; spray voltage 3.2 kV; S-Lenses RF level, 69%. Scan range was 100–2000 *m*/*z*. Fragmentation was performed by chemical induced dissociation (CID) at the linear trap. The data were analysed using Xcalibur 4.1 (Thermo Fisher Scientific). Aqueous 50 μM solutions of βCD and CB7 hosts were prepared and infused. The studies of the presence of aqueous phase complexes were performed by adding 2–3 mg of **1** to 5 mL of these host solutions. The non-soluble particles of **1** were allowed to settle down and the aqueous phase was then infused. For comparison purposes, **1** was mixed with water in the same way but without any host.

Myoglobin assay

CO release from complex **1**, **1**@βCD(IP) and **1**@CB7 was studied spectrophotometrically and quantified by the myoglobin (Mb) assay which uses absorption spectroscopy to follow the conversion of deoxy-Mb to carbonmonoxy-Mb (MbCO).[53,66] The amount of MbCO formed over time was determined by periodically recording absorption spectra and monitoring changes in the Q-band region, *i.e.*, the loss of the absorption band with λ_{max} = 557 nm due to deoxy-Mb, and the concomitant appearance of bands with λ_{max} = 540 and 577 nm due to MbCO.

Stock solutions of Mb (~100 μM) and sodium dithionite (10, 20 or 40 mg mL^{-1}) were freshly prepared in N_2-degassed 10 mM PBS or HEPES buffer (pH 7.4). Under an atmosphere of nitrogen, the stock solutions were added to a sealed semi-micro (3500 μL) quartz cuvette (containing a magnetic stirring bar) in the following order: 10 mM PBS (1185 μL), 100 μM Mb (1500 μL), sodium dithionite solution (300 μL). A spectrum of the resultant solution was recorded to capture the deoxy-Mb profile (0% MbCO). Subsequently, an aliquot (15 μL) of a freshly prepared 4 mM solution of **1** or the CD/CB adducts in N_2-degassed DMSO or ethanol was added to the cuvette to give a final concentration of 20 μM. The quartz cell was kept either in the dark or exposed to UV light (λ = 365 nm), at 37 °C, with constant magnetic stirring at 400 rpm.

The assays were conducted over a period of either 30 min (for initial dithionite concentrations of 0.1% and 0.2%) or 6 h (for an initial dithionite concentration of 0.4%), interrupting the incubation in intervals of either 10 min or 30 min to measure absorption spectra of the sample between 450 and 650 nm, using a scan speed of 200 nm min^{-1} and a slit width of 2 nm. At the end of each assay, the sample was converted to 100% MbCO by bubbling CO gas through the liquid phase for 5 min, and an absorption spectrum was recorded. The actual concentration of Mb in the cell ([Mb] = 38–48 μM) was then determined by using the known extinction coefficient of MbCO at 540 nm (15.4 mM^{-1} cm^{-1}).[67] The assays were carried out in duplicate or triplicate, and the spectroscopic data were treated in the standard way by applying a correction at the 510 nm isosbestic point.[66]

Results and discussion

Synthesis and solid-state characterisation

Fig. 2 illustrates the three synthetic methods employed in this work. In each case a starting **1** : βCD or **1** : CB7 stoichiometry of 1 : 1 was used. Two different solution-based precipitation techniques were used. For βCD, mixing of an aqueous solution of the host with a solution of **1** in dichloromethane resulted in the formation of a pale-yellow precipitate, designated as **1**@βCD(IP). This liquid–liquid interfacial precipitation (IP) method works particularly well for the isolation of inclusion compounds between βCD and organometallic guests, especially metallocene and half-sandwich cyclopentadienyl complexes that are insoluble, or only sparingly soluble, in water.[55,68,69] To isolate the CB7 adduct, the liquid antisolvent precipitation method was used, which in its simplest form involves dissolution of a poorly water-soluble drug in a solvent (in which it is highly soluble), which is then mixed with a miscible antisolvent (in which the drug is poorly soluble).[70] If desired, an excipient may be dissolved in either the antisolvent or the same solvent as the drug. This energy-efficient technique is of interest to the pharmaceutical industry due to its simplicity, low cost, and scalability. For CB7 and **1**, a pale-yellow precipitate (denoted as **1**@CB7) was obtained upon addition of water (as antisolvent) to a solution of **1** and CB7 in ethanol, as described recently in a study of the use of the inclusion compound as a supramolecular precatalyst for the epoxidation of olefins.[61]

From an industrial perspective, improving the aqueous solubility of poorly water-soluble drugs by co-grinding in the

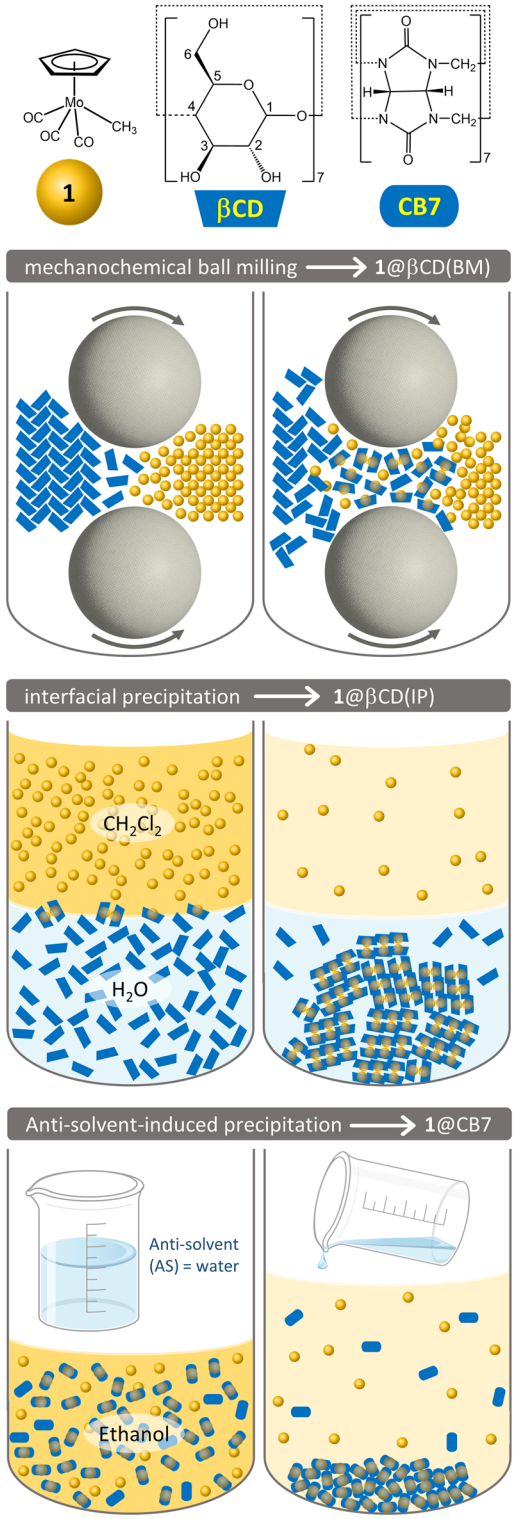

Fig. 2 Schematic representations of the synthetic methods used in the present work.

dry state with a suitable excipient is very appealing.[71] Co-grinding of drug/cyclodextrin physical mixtures in different types of mills has been demonstrated to be an eco-friendly solvent-free approach for mechanochemical activation of the sample and possible inclusion complexation in the solid state.[72] This method was explored in the present work by co-grinding a **1**/βCD mixture in a planetary ball mill, which resulted in the solid denoted as **1**@βCD(BM). The solids **1**@βCD(IP), **1**@βCD(BM) and **1**@CB7 were characterised in the solid state by TGA, PXRD, FT-IR spectroscopy, and $^{13}C\{^1H\}$ CP MAS NMR spectroscopy.

Fig. 3 shows the TGA curves of **1**, the native hosts βCD and CB7, and the CORM@(βCD/CB7) compounds (measured under air). Complex **1** shows two main weight loss steps from room temperature up to 530 °C: a mass loss of 48.6% between 80 and 180 °C (DTG peak at 157 °C), and a loss of 8.0% between 470 and 525 °C (DTG peak at 500 °C). The low final residual mass of 33.1% indicates that a combination of decomposition and sublimation took place during the experiment, probably during the first weight loss step, *i.e.*, decarbonylation of **1** may occur simultaneously with sublimation of the complex. βCD hydrate starts to melt and decompose at about 270 °C, and two steps are observed up to 550 °C (DTG peaks at 315 and 488 °C), at which point the mass loss is 100%. The well-defined weight loss of 14.1% from room temperature up to 140 °C (DTG peak at 104 °C) is assigned to removal of water molecules located in the βCD cavities and in the interstices between the macrocycles (*ca.* 10.5 water molecules per βCD molecule). The TGA curves for **1**@βCD(IP) and **1**@βCD(BM) are similar up to the main decomposition event (DTG peak at 240 °C for **1**@βCD(IP), 254 °C for **1**@βCD(BM)). For both compounds, this step is preceded by a minor inflection at about 190 °C (more easily discerned for **1**@βCD(IP)) which is associated with a faint DTG peak at about 172 °C. Since this feature is not observed for native βCD, we attribute it to a mass loss stemming from decarbonylation/sublimation of tricarbonyl complex. Further mass loss associated with included complex is suggested to take place concomitantly with decomposition

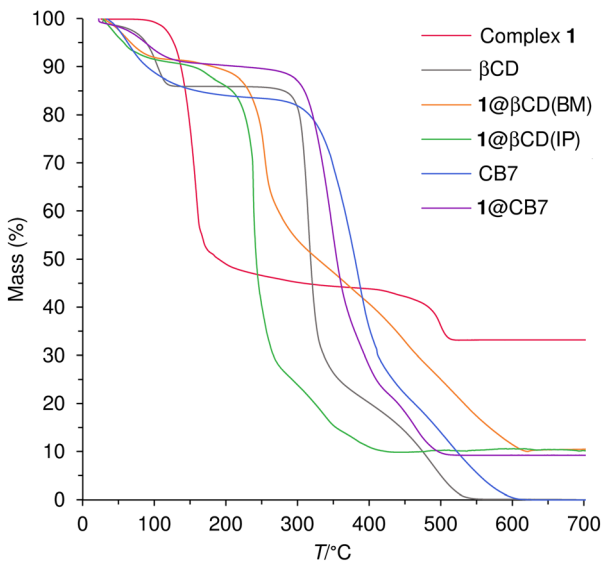

Fig. 3 TGA curves of **1**, βCD, CB7, **1**@βCD(BM), **1**@βCD(IP) and **1**@CB7.

of the cyclodextrin. The promoting effect of Mo on the decomposition of βCD is evidenced by the shift of the macrocycle decomposition from around 315 °C for native βCD to around 250 °C for the inclusion compounds. The main difference between the TGA curves for **1**@βCD(IP) and **1**@βCD(BM) is that the latter displays a more protracted mass loss above 260 °C, with a plateau only being reached at 625 °C. Despite this difference, the TGA results are very similar regarding the initial water loss step (8.6–9.3% in the range 28–130 °C) and final residual mass (10.4% at 650 °C). Considering that the residue at 650 °C is MoO_3, these values are close to the calculated ones for the net molar composition of **1**·βCD·7.5H_2O (calcd: H_2O, 8.8%; MoO_3, 9.4%).

The TGA curves of native CB7 and **1**@CB7 are similar except that the latter displays a lower mass loss due to removal of water (and a small amount of acetone) between room temperature and 200 °C (9.8% *vs.* 16.0%), and a non-zero residual mass (9.2%) at 650 °C. These values are consistent with the net molar composition of **1**·CB7·9H_2O (calcd: H_2O, 10.2%; MoO_3, 9.1%). In the temperature range of 100–275 °C, the TGA curve of **1**@CB7 does not exhibit any weight loss step that could be due to sublimation/decarbonylation of **1** (either "free" or encapsulated). Hence, sublimation/decarbonylation of **1** is inhibited by full encapsulation by the CB7 host, with the oxidative decomposition of the organometallic guest taking place concurrently with cucurbituril decomposition above 275 °C (a single DTG peak is observed at 348 °C; *cf.* native CB7, which exhibits a single DTG peak at 385 °C). These results provide good support for the presence of a true inclusion compound in which the [$CpMo(CO)_3Me$] molecules are tightly encapsulated within the CB cavity.

PXRD patterns are shown in Fig. 4. By comparing the patterns for **1**@βCD(IP) (Fig. 4c) and microcrystalline **1** (Fig. 4a), the presence of the latter (*i.e.*, nonincluded **1**) can be excluded. The pattern for **1**@βCD(IP) is distinct from that for βCD (Fig. 4b) and closely resembles (in terms of the angular positions of peaks) the reference patterns published for two isostructural series of dimeric βCD inclusion complexes crystallising in the space groups *P*1 (triclinic) and *C*2 (monoclinic).[73] Fig. 4d shows the reference pattern for the *C*2 set of complexes. As explained by Caira and co-workers,[74] a definitive assignment of an inclusion complex to the space group *P*1 or *C*2 is not possible from PXRD alone since the calculated PXRD patterns for two structures containing the same dimeric βCD inclusion complex are virtually indistinguishable. In both isostructural series, complex units pack in the channel mode, characterised by close-packed layers of βCD dimers stacked in alignment to produce channels. A very similar PXRD trace was obtained previously for the inclusion complex between βCD and [$CpMo(CO)_3Cl$].[55] Hence, the PXRD pattern for **1**@βCD(IP) proves that a genuine inclusion complex is formed. Fig. 5 shows a schematic model of the possible structure of the inclusion compound **1**@βCD(IP) based on channel-type packing of head-to-head βCD dimers containing encapsulated organometallic guest molecules.

The PXRD pattern of **1**@βCD(BM) (Fig. 4e) reveals two very weak and broad peaks centred at *ca.* 6.1° and 11.6° 2θ, and a much more intense broad hump centred at *ca.* 17.7° 2θ. Sharp peaks superimposed on the amorphous peak correspond to those displayed by crystalline **1** (Fig. 4a), indicating that the sample contains some nonincluded complex. On the other

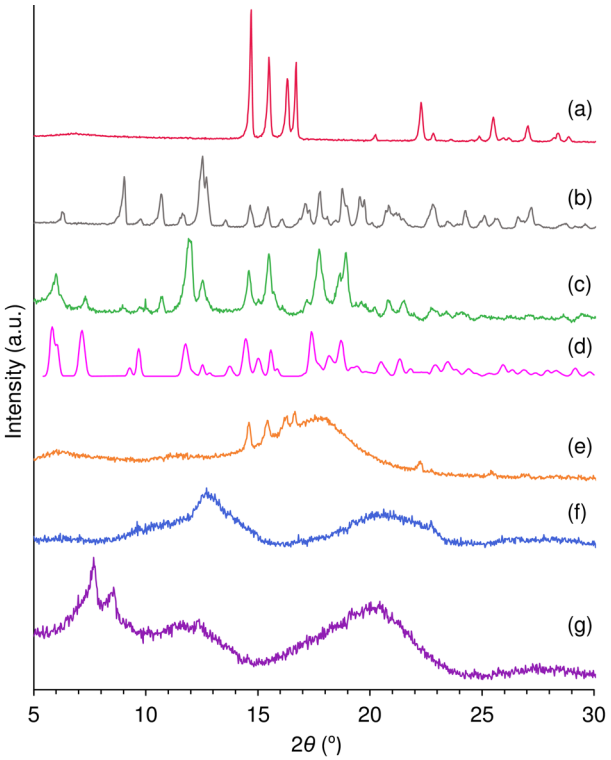

Fig. 4 Experimental PXRD patterns of (a) **1**, (b) βCD, (c) **1**@βCD(IP), (e) **1**@βCD(BM), (f) CB7, and (g) **1**@CB7. The reference pattern for the isostructural series of βCD inclusion complexes with space group *C*2 is shown in (d).[73]

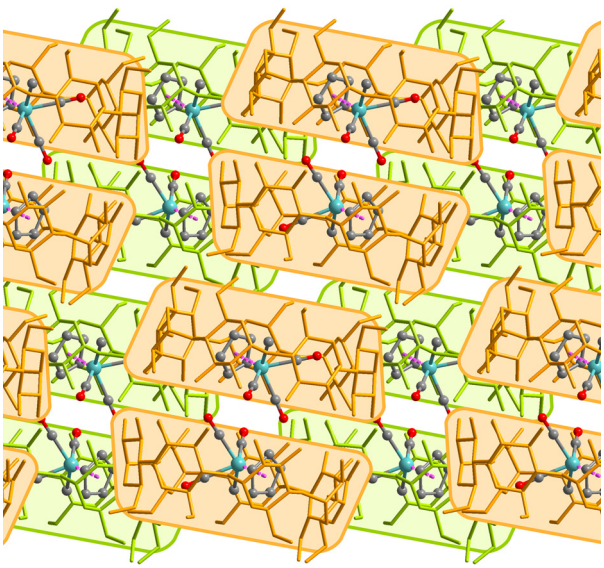

Fig. 5 Schematic model of the possible structure of the inclusion compound **1**@βCD(IP) based on channel-type packing of complex units.

hand, the pattern does not contain reflections characteristic of crystalline native βCD hydrate (Fig. 4b). Hence, the grinding process either induced complete amorphisation of βCD or complexation with **1** to give an essentially amorphous inclusion compound. The latter scenario is supported by the fact that the PXRD trace for the X-ray amorphous phase follows the intensity envelope observed in the powder pattern of **1**@βCD(IP). The presence of some nonincluded **1** in **1**@βCD(BM) is not unexpected given that co-grinding with crystalline CDs frequently leads to only partial drug complexation, *i.e.*, the products contain a fraction of residual crystalline drug.[72] From a practical viewpoint, this may not be important because it has been demonstrated that the dissolution rate of nonincluded drug components in such products is often greatly improved with respect to that of the pure drug, which has been attributed to inclusion complex formation upon dissolution.[72]

PXRD confirmed the amorphous nature of the as-synthesised CB7 sample (Fig. 4f). It is noteworthy, however, that the trace matches with the intensity envelope observed in the PXRD pattern of a more crystalline CB7 sample reported previously,[75] indicating that the two samples have the same basic structure (cucurbituril packing arrangement), albeit with different degrees of long-range order. The compound **1**@CB7 also produced a halo pattern characteristic of an amorphous solid. This pattern is, nevertheless, different from that for CB7 in that two sharper peaks are observed at 7.7° and 8.5° 2θ, possibly indicating a different packing arrangement for the host molecules and hence the presence of a genuine inclusion complex with **1**.

The ATR FT-IR and FT-Raman spectra of **1**@βCD(BM), **1**@βCD(IP) and **1**@CB7 contain the characteristic bands of the macrocyclic host molecules, with no significant shifts being registered (Fig. 6). The ATR FT-IR spectra show two bands in the CO stretching region at 1921–1929 cm^{-1} and 2012–2016 cm^{-1}. The bands are shifted to higher frequency by 31–39 cm^{-1} and 9–13 cm^{-1}, respectively, relative to those for non-included complex **1** in the solid state. It is also noteworthy that the shape of the lower-frequency ν_{CO} band changes from being very broad and asymmetric for **1** (with an extended shoulder on the low-frequency side) to relatively sharp and symmetric for **1**@βCD(BM), **1**@βCD(IP) and **1**@CB7. These spectral changes are consistent with inclusion complexation. Thus, the asymmetric broadening of the ν_{CO} band for **1** may be due to solid-state intermolecular interactions (CH···O and CH···π contacts, which are known to be present in carbonyl/Cp-containing organometallics[76]), which would not be present for the inclusion compounds. Secondly, the blue shifts observed for the ν_{CO} bands of **1**@βCD(BM), **1**@βCD(IP) and **1**@CB7 mirror those typically observed when comparing solution and solid-state FT-IR spectra of organomolybdenum carbonyl complexes, thereby indicating that the organometallic guest complexes are in a "solution-like" isolated environment by encapsulation in the host cavities.[68,69] Similar blue shifts are observed for the Raman ν_{CO} bands: from 1904 and 2006 cm^{-1} for **1** to 1927–1934 cm^{-1} and 2017–2019 cm^{-1} for the inclusion compounds.

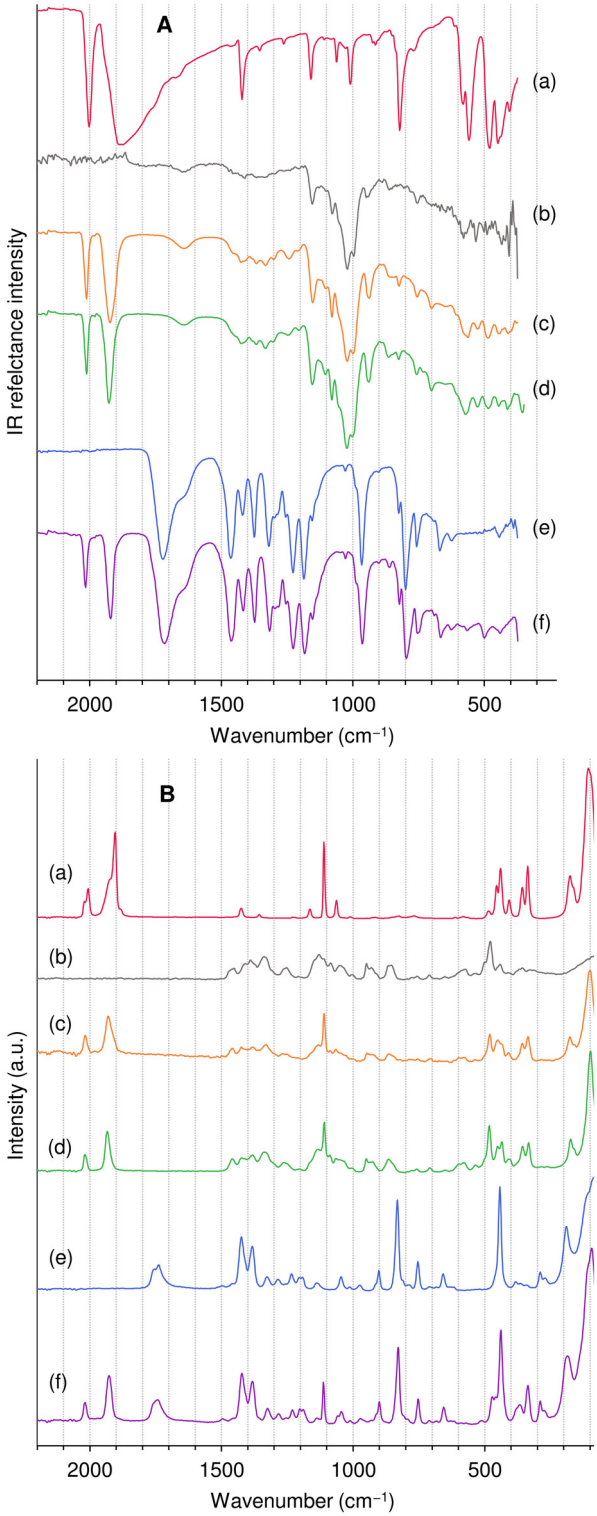

Fig. 6 ATR FT-IR (A) and FT-Raman (B) spectra of (a) **1**, (b) βCD, (c) **1**@βCD(BM), (d) **1**@βCD(IP), (e) CB7, and (f) **1**@CB7.

The $^{13}C\{^{1}H\}$ CP MAS NMR spectra of **1**@βCD(BM), **1**@βCD(IP) and **1**@CB7 are shown in Fig. 7, along with those for pure **1** and the native host macrocycles. βCD hydrate displays multiple sharp lines for each type of chemically equivalent carbon

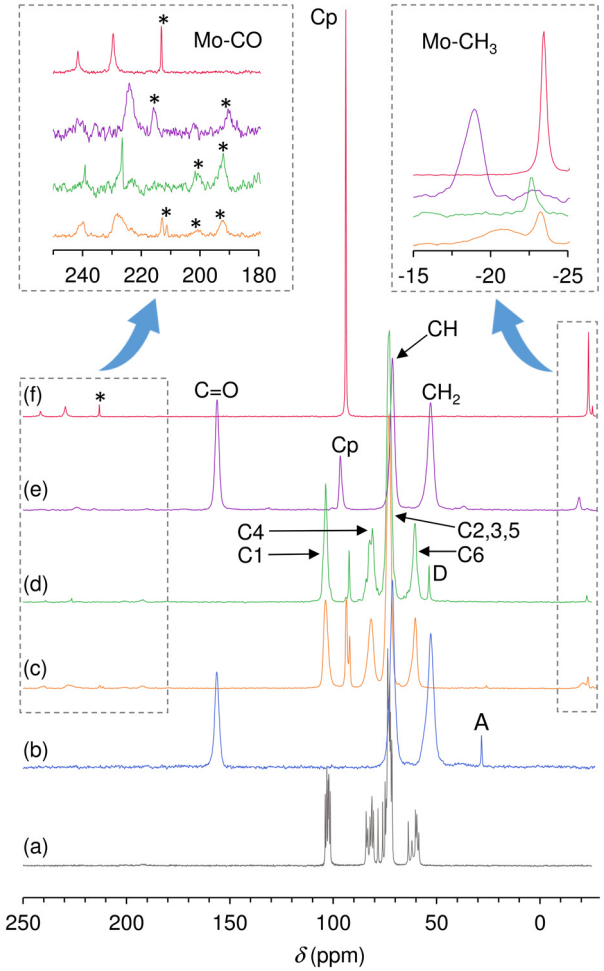

Fig. 7 $^{13}C\{^1H\}$ CP MAS NMR spectra of (a) βCD hydrate, (b) CB7, (c) **1**@βCD(BM), (d) **1**@βCD(IP), (e) **1**@CB7, and (f) **1**. Amplifications of the Mo–CO and Mo–CH_3 regions are shown for spectra (c) to (f), and representative assignments are indicated for spectra (d) to (f). Fig. 2 shows the carbon atom numbering for βCD. The asterisks denote spinning sidebands, A denotes acetone resonance, and D denotes CH_2Cl_2 resonance.

atom (C1–C6), with the peaks for C1, C4 and C6 being spread over the chemical shift range of 3–6 ppm (Fig. 7a). This has been attributed to the fact that, in the crystalline state, the macrocycle does not have complete cylindrical symmetry, *i.e.*, the carbon atoms become magnetically inequivalent due to different torsion angles about the α-1,4-glycosidic linkages, and rotation about the C5–C6 bond which leads to different hydrogen bonding interactions.[77] In the spectra of **1**@βCD (BM) and **1**@βCD(IP), the carbons C1, C6 and C2,3,5 (and also C4 for **1**@βCD(BM)) give rise to single peaks (Fig. 7c and d). This frequently observed effect has been attributed to the inclusion-induced symmetrisation of the cyclodextrin such that each glucose unit is in a similar environment. In addition to the resonances for the βCD carbons, the spectra of **1**@βCD (BM) and **1**@βCD(IP) exhibit several resonances that can be assigned to the carbon atoms of the guest molecule. For **1**@βCD(BM), two sharp peaks are observed for the η^5-cyclopentadienyl ring at 92.0 and 93.6 ppm, the latter of which coincides with the single resonance observed for **1** in the solid-state ^{13}C NMR spectrum (Fig. 7f). Similarly, the relatively sharp peak at −23.2 ppm matches the Mo–CH_3 chemical shift of −23.4 ppm for **1**, while a second broader and weaker signal at −20.8 ppm is attributed to encapsulated complexes. The compound **1**@βCD(IP), on the other hand, only displays single Mo-CH_3 and Cp lines at −22.6 and 92.2 ppm, which are assigned to encapsulated tricarbonyl complexes. In the solid-state ^{13}C NMR spectrum of **1**, the carbonyl resonances appear as two sharp peaks, one at 229.6 ppm for the two *syn* carbonyls and a weaker one at 241.6 for the *trans* carbonyl, in agreement with that reported previously.[78] Hence, although the two *syn* carbonyl carbon atoms are crystallographically inequivalent,[79] no inequivalence in the chemical shifts is observed. The two inclusion compounds present a similar pattern of carbonyl resonances, except that the peaks are shifted upfield by 1.8–3.1 ppm. The two resonances are sharp for **1**@βCD(IP), and relatively broad for **1**@βCD(BM). Overall, the $^{13}C\{^1H\}$ CP MAS NMR spectra of **1**@βCD(BM) and **1**@βCD(IP) support the presence of real inclusion complexes, while also appearing to fit with the PXRD results for **1**@βCD(BM) in revealing the presence of nonincluded **1**.

The $^{13}C\{^1H\}$ CP MAS NMR spectrum of **1**@CB7 shows single relatively sharp peaks for the guest molecule, shifted either downfield (from −23.5 to −18.9 ppm, and from 93.9 to 96.6 ppm) or upfield (from 229.5 to 224.2 ppm) relative to those for **1** (Fig. 7b, e and f). Regarding the signals for the CB7 carbons, the spectra of CB7 and **1**@CB7 are practically identical, showing single peaks centred at 156.1 ppm for the C═O groups, 71.3 ppm for the CH groups, and 52.9 ppm for the bridging CH_2 groups.

Host–guest complexes in aqueous solution

Mass spectrometry has contributed only rarely to the characterisation of inclusion complexes between cyclopentadienyl metal complexes and macrocyclic hosts such as CDs and CBs.[80] Nevertheless, a few studies have shown that ESI-MS can be useful as a complementary approach to study noncovalently bound host–guest complexes involving organometallic guests such as ferrocene derivatives and titanocene dichloride.[80–83] In the present work, the formation of aqueous phase complexes was studied by ESI-HRMS as this technique shows much higher sensitivity than NMR. An ethanolic solution of **1** in the absence of host was analysed first. Very few signals were detected. However, a series of very weak peaks, compatible with the isotope distribution of Mo, was observed between *m*/*z* 230 and 250 (Fig. S2†). This isotope series, which is a signature of the presence of Mo in the ion structure, is compatible with the formula $C_7H_{11}O_3^+$. The low intensity of the signals prevented us from obtaining further insights into this structure. Fig. S3† presents the spectrum of an aqueous solution of CB7 (50 μM), showing a base peak at *m*/*z* 604.161 corresponding to the doubly charged sodiated CB7, $[CB7 + 2Na]^{2+}$.[84] The addition of solid **1** to this solution gave rise to a new strong

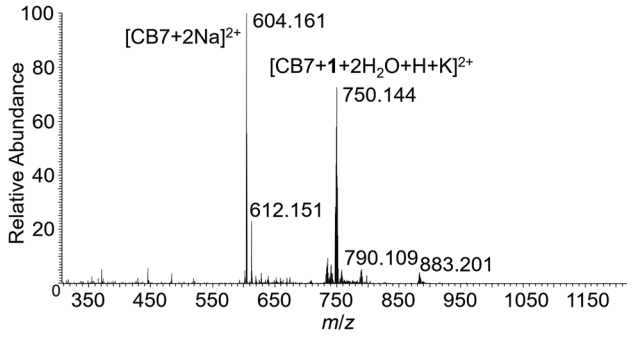

Fig. 8 ESI-HRMS full scan spectrum of **1**@CB7.

signal peaking at 750.144 (Fig. 8). The isotope distribution indicates the presence of Mo in a doubly charged structure ($\Delta m/z$ = 0.5, see Fig. S4†). Analysis of the isotope distribution indicates this signal is compatible with the formula $C_{51}H_{55}MoN_{28}O_{19}K^{2+}$ (Fig. S4†), which fits with the ion [CB7 + **1** + $2H_2O$ + H + K]$^{2+}$ (Fig. 8). The analysis of the CID spectra revealed the loss of water and carbonyls, in agreement with the proposed structure (Fig. S5†). The results suggest CB7 is forming host–guest complexes with intact **1**. Although the preparation procedure of **1**@CB7 involves its precipitation with water (Fig. 2), the aqueous solubility of these complexes is high enough for detection by ESI-HRMS. No signals assignable to complexes were detected in solutions with βCD and **1** (Fig. S6†).

Stability of 1

The stability of **1** was investigated in the solid state and in solution. To assess the stability in the solid state, ATR FT-IR spectra were periodically recorded over a period of 28 days for a sample exposed to ambient air and light (Fig. S7†). The results indicate that the compound is fairly stable for up to about 2 weeks, but spectral changes thereafter indicate that decomposition begins to take place, with the loss of the ν_{CO} bands pointing to extensive decarbonylation. For the solution studies, **1** was dissolved in degassed DMSO or EtOH, and UV-vis spectra were periodically recorded over a period of 6 h (Fig. S8†), maintaining the solutions in the dark. In both solvents, **1** displays one absorption band at 314 nm, in excellent agreement with literature data (315 nm in cyclohexane).[63] The absence of measurable spectral changes over 6 h confirmed the high stability of solutions of **1** in these solvents, which were therefore chosen as delivery media for the Mb assays. An additional test was performed in which a solution of **1** in DMSO was exposed to UV light (365 nm, E = 2.5 mW cm^{-2}) over 2 h. Major spectral changes were observed within 30 min for the irradiated solution (Fig. S9†), with the almost complete loss of the band initially present at 314 nm. It is presumed that these alterations stem from photodecarbonylation of **1** since it is known, for example, that irradiation of hydrocarbon solutions of **1** with UV light in the presence of a coordinating solvent or ligand (L) can lead to both monosubstituted and di-substituted derivatives, [CpMo(CO)$_2$(L)Me] and [CpMo(CO)(L)$_2$Me].[62,85]

CO release studies

The CO release behaviours of **1**, **1**@βCD(IP) and **1**@CB7 were evaluated by the standard Mb assay using UV-vis spectroscopy. The first assays with **1** were performed to determine the influence of the buffer. In these assays, freshly prepared Mb from equine skeletal muscle was added to degassed 10 mM PBS or HEPES solutions and then reduced with an excess (0.4%) of sodium dithionite, under nitrogen atmosphere. A solution of **1** in DMSO was added to the former solution and stirred at 37 °C in the dark. Under these conditions, CO release reached a plateau for both buffers (at 2 h), with the amounts of 1.61 mol of CO per mol of complex using HEPES, and 1.49 mol CO per mol of complex using PBS (Fig. S10 and S11†). Although the results for the two buffers are similar, PBS was chosen for all subsequent assays since it mimics the ion concentration, osmolarity, and pH of human body fluids. In other words, PBS is isotonic to human solutions, being non-toxic and preventing cell damage or undesirable precipitation in biological and biomedical research.

To study the effect of the delivery solvent on the CO release from **1**, a Mb assay (10 mM PBS buffer) was performed in which **1** was dissolved in degassed EtOH rather than DMSO. The decarbonylation levelled out at 1.64 mol CO per mol complex after 90 min of incubation in the dark (Fig. S11(B)†), which is slightly higher than the value of 1.49 mol CO per mol of complex determined with a DMSO solution as the delivery medium (Fig. S10†). The half-lives ($t_{1/2}$) of CO-release, defined as the time taken for a solution of CORM with a concentration of X μM to produce a solution of MbCO with a concentration of X/2 μM,[66] were 25 min with DMSO, and 16 min with EtOH.

A recognised drawback of the Mb assay is that CO release from a CORM may be induced by reaction with sodium dithionite, which must be present in excess (relative to Mb) to reduce Mb to deoxy-Mb. This has been shown to be the case with two of the earliest and most studied metal carbonyl CORMs, [Ru(CO)$_3$Cl$_2$]$_2$ (CORM-2) and [Ru(CO)$_3$Cl(glycinate)] (CORM-3), which were originally identified as fast CO releasers based on the Mb assay, but were later shown to be very slow releasers in the absence of dithionite.[86,87] In the present work, two modified Mb assays were performed with **1** to assess the influence of dithionite on the release of CO (both with DMSO as the delivery solvent). In the first assay, **1** was incubated in the dark in PBS buffer and sodium dithionite (0.4%) for 30 min, followed by addition of Mb. As expected (based on the normal assay, Fig. S10(A)†), there was an immediate leap in MbCO formation (corresponding to 0.50 mol_{CO} $mol_{complex}^{-1}$), and CO continued to be released as the assay progressed, reaching 1.11 mol_{CO} $mol_{complex}^{-1}$ after 3 h (Fig. S12†), which is only slightly lower than the 1.49 equiv. reached in the normal assay. In the second assay, **1** was incubated in the dark in PBS alone for 30 min, followed by addition of Mb and dithionite (0.4%). Only a minor amount of MbCO was registered at this point (0.03 mol_{CO} $mol_{complex}^{-1}$), indicating that very little CO

was released from **1** during the initial 30 min incubation in PBS at 37 °C. On the other hand, the MbCO concentration started to increase in an approximately linear fashion after the addition of dithionite and Mb, reaching 0.46 mol_{CO} $mol_{complex}^{-1}$ after 3 h, which indicates that CO release from **1** is facilitated by dithionite.

To further study the influence of dithionite on CO release from **1**, Mb assays were performed with lower amounts of the reducing agent (0.2% and 0.1%; the latter corresponds to 140 equivalents relative to Mb). The incubation time for these assays was restricted to 30 min since it was found that the lower amounts of dithionite compromised the stability of deoxy-Mb over the course of the assay, *i.e.*, longer incubation times led to increasing oxidation of deoxy-Mb (Fe^{2+}) to met-Mb (Fe^{3+}), evidenced by the appearance of a LMCT (ligand-to-metal charge transfer) band in the range of 600–650 nm. In accordance with the assays described above, decreasing the amount of dithionite resulted in lower CO release rates. The higher amount of dithionite (0.4%) led to an initial MbCO formation rate of 23.6 μM h^{-1} (based on the MbCO concentration at 30 min, which equated to 0.59 mol_{CO} $mol_{complex}^{-1}$). For the lower amounts of dithionite, MbCO concentrations increased almost linearly during 30 min with rates of 9.6 μM h^{-1} for 0.2% (R^2 = 0.999; 0.24 mol_{CO} $mol_{complex}^{-1}$ at 30 min), and 2.3 μM h^{-1} for 0.1% (R^2 = 0.996; 0.06 mol_{CO} $mol_{complex}^{-1}$ at 30 min) (Fig. 9). Thus, a 4-fold decrease in the amount of dithionite led to a 10-fold decrease in the CO release rate.

It is pertinent to compare the CO release behaviour of **1**, measured by the Mb assay, with data reported by Lynam and co-workers for the complex $[CpMo(CO)_3Cl]$.[33] Under similar conditions (DMSO delivery medium, CORM concentration of 20 μM, 10 mM PBS, pH 7.4, 37 °C, 0.1% dithionite, in the dark), the chloro complex exhibited relatively fast and sustained CO release over the course of 30 min, with a half-life of 14.4 min, whereas complex **1** is a very slow releaser, as described above. Lynam and co-workers did not mention whether tests were performed to screen for dithionite dependence.

Considering the known propensity of complex **1** to undergo photodecarbonylation, together with the results of the photostability study performed in the present work, Mb assays were carried out to establish the potential of **1** to act as a photoactivatable CORM (photoCORM). Dithionite-promoted CO release was minimised by using lower amounts of the reducing agent. Solutions of **1** with a concentration of 20 μM were prepared and exposed to UV light of wavelength 365 nm from a 15 W lamp. This resulted in a far more rapid and significant release of CO when compared with the dark reactions, with a half-life of 6.3 min for assays carried out with 0.1% and 0.2% dithionite (Fig. 9). For the two assays, MbCO concentrations only started to diverge after 10 min, reaching (at 30 min) 23.4 μM (1.17 equiv.) for the 0.1% dithionite assay, and 28.6 μM (1.43 equiv.) for the 0.2% assay. The difference of 0.26 equiv. is attributed to two factors: (i) partially enhanced dithionite-promoted CO release with 0.2% dithionite (the difference was 0.18 equiv. for the assays carried out in the dark with 0.1% and 0.2% dithionite); (ii) higher interference from the oxidation of deoxy-Mb to met-Mb in the case of the lower dithionite concentration.

The photodecarbonylation behaviour of **1** seems to be quite similar to that reported previously for the alkynyl complex $[CpMo(CO)_3(C{\equiv}CCH_2R)]$ containing a β-D-fructopyranose group (R).[33] Under similar conditions to those employed for **1** (DMSO delivery medium, CORM concentration of 20 μM, 10 mM PBS, pH 7.4, 37 °C, 0.1% dithionite, irradiation with a 6 W UV lamp (325 nm)), the alkynyl complex exhibited a half-life of 13 min, and resulted in the formation of an MbCO concentration of 25 μM after 30 min.

Although using EtOH as the delivery solvent for **1** in the Mb assay (with 0.4% dithionite) led to the best results (in terms of maximum amount of CO released), the Mb assays for **1**@βCD (IP) and **1**@CB7 were performed using DMSO due to solubility

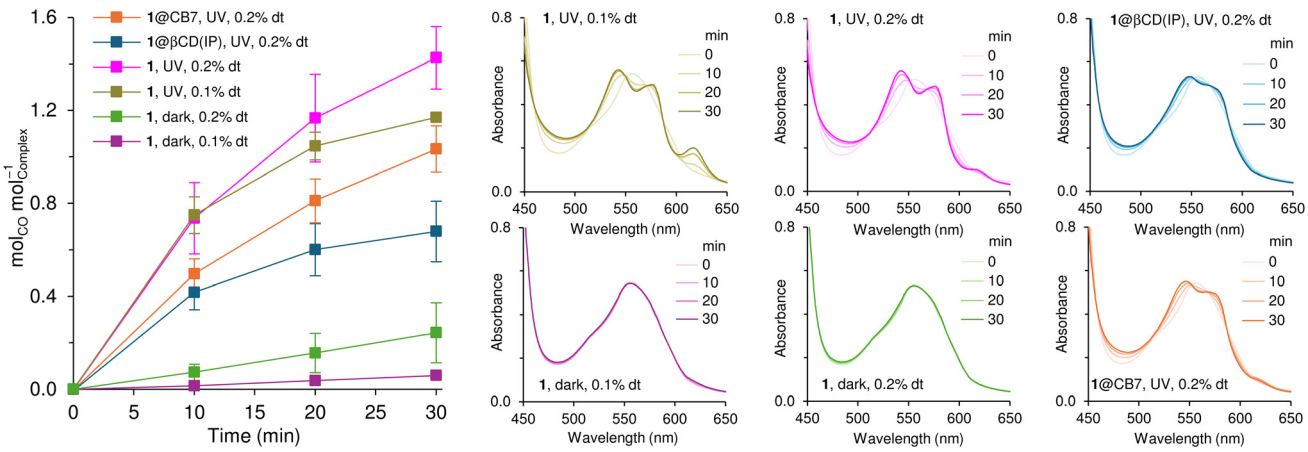

Fig. 9 UV-vis spectra (Q-band region) and resultant CO release profiles obtained from Mb assays performed at 37 °C with 20 μM solutions of **1**, **1**@βCD(IP) and **1**@CB7, either in the dark or with UV light irradiation, and with different amounts of dithionite (dt) reducing agent. The data values are the mean ± standard deviation of two independent assays.

constraints in ethanol (both compounds were insoluble in EtOH, while **1**@βCD(IP) was soluble in DMSO, and **1**@CB7 was partially soluble in DMSO). The pristine hosts, βCD and CB7, were chosen as negative controls and tested in a DMSO/PBS mixture, with a final concentration of 20 μM in the deoxy-Mb mixture (0.4% dithionite, in the dark). As expected, neither host produced any change in the UV-vis absorption spectrum of deoxy-Mb over an assay duration of 6 hours.

To study the photochemically activated CO release from **1**@βCD(IP) and **1**@CB7, Mb assays were performed as described above for **1** with 20 μM solutions, 0.2% dithionite, and exposure to UV light (λ = 365 nm). The assays confirmed the retention of photoactivatable CO release for the encapsulated complex, albeit with slightly lower CO release rates, as revealed by the half-lives of 13.2 min for **1**@βCD(IP) and 10 min for **1**@CB7, and the number of molecules of CO released per complex after 30 min (*ca.* 0.7 and 1, respectively, Fig. 9).

In Mb assays performed in the dark with 0.4% dithionite, CO release from **1**@βCD(IP) reached a maximum of 0.37 mol_{CO} $mol_{complex}^{-1}$ at 4.5 h (Fig. S10(A)†). **1**@CB7 presented a similar profile but with enhanced decarbonylation, reaching 1.0 mol_{CO} $mol_{complex}^{-1}$ at 3.5 h. The $t_{1/2}$ for the latter was 43 min. Since 0.5 equivalents of CO were not released from **1**@βCD(IP) over the course of the assay, $t_{1/2}$ cannot be determined. For comparison purposes, $t_{1/4}$ can be employed instead,[66] and the corresponding values are *ca.* 13 min for **1**, 120 min for **1**@βCD(IP), and 19 min for **1**@CB7. These results can be explained by the presence of intact **1**@βCD inclusion complexes in solution in the case of **1**@βCD(IP), with the host macrocycle protecting the encapsulated organometallic complex from the surrounding aqueous medium containing excess dithionite, thereby resulting in a strongly attenuated release of CO. The ESI-HRMS studies for **1**@CB7 confirmed the formation of host–guest complexes in aqueous medium. It seems, therefore, that CB7 is less capable than βCD in protecting encapsulated **1** from CO release induced by reaction with the reducing agent sodium dithionite.

Conclusions

In the present work, we have shown that coprecipitation from solution allows the isolation of true inclusion compounds between the complex [$CpMo(CO)_3Me$] (**1**) and βCD or CB7. Inclusion complexation between **1** and βCD can be induced by solid-state co-grinding, although characterisation of the resultant product indicated the presence of some nonincluded complex. Mb assays have shown that complex **1** releases CO through reaction with the reducing agent sodium dithionite and/or photoactivation after exposure to UV light, with the latter process assuming dominance when lower amounts of dithionite are used. The CO release profiles for the inclusion compounds show that these macrocyclic hosts offer considerable potential for modulating CO-release behaviour. βCD had the largest effect on the CO-release rates, which can be attributed to the propensity of CDs to form stable inclusion compounds with sandwich (cyclopentadienyl) complexes of molybdenum. In conclusion, this work validates the use of CDs and CBs to prepare CORM-carrier conjugates that may improve the bioavailability of neutral organometallic photoCORMs and the delivery of CO to biological targets.

Author contributions

Rodrigo P. Monteiro: methodology, validation, investigation, writing – original draft, writing – review & editing, visualisation. Isabel B. Calhau: methodology, validation, investigation, writing – original draft, writing – review & editing, visualisation. Ana C. Gomes: methodology, validation, investigation, writing – original draft, writing – review & editing, visualisation. André D. Lopes: methodology, validation, investigation, resources, writing – review & editing. José P. Da Silva: methodology, validation, formal analysis, investigation, resources, writing – original draft, writing – review & editing. Isabel S. Gonçalves: conceptualisation, resources, writing – review & editing, supervision, funding acquisition. Martyn Pillinger: conceptualisation, resources, writing – review & editing, visualisation, supervision, funding acquisition.

Data availability

The data that support the findings of this study are available in the main article, the ESI,† and from the corresponding authors upon reasonable request.

Conflicts of interest

There are no conflicts to declare.

Acknowledgements

This work was developed within the scope of the project CICECO-Aveiro Institute of Materials, UIDB/50011/2020 (**https://doi.org/10.54499/UIDB/50011/2020**), UIDP/50011/2020 (**https://doi.org/10.54499/UIDP/50011/2020**) & LA/P/0006/2020 (**https://doi.org/10.54499/LA/P/0006/2020**), financed by national funds through the FCT (Fundação *para* a Ciência e a Tecnologia)/MCTES (Ministério da Ciência, Tecnologia e Ensino Superior) (PIDDAC). This study received Portuguese national funds from the FCT through projects UIDB/04326/2020 (**https://doi.org/10.54499/UIDB/04326/2020**), UIDP/04326/2020 (**https://doi.org/10.54499/UIDP/04326/2020**) and LA/P/0101/2020 (**https://doi.org/10.54499/LA/P/0101/2020**), and from the operational programmes CRESC Algarve 2020 and COMPETE 2020 through project EMBRC.PT ALG-01-0145-FEDER-022121. R.P.M. (**https://doi.org/10.54499/2020.04758.BD**) and I.B.C. (**https://doi.org/10.54499/2021.05953.BD**) are grateful to the FCT and the European Social Fund for PhD

grants. A.C.G. acknowledges the FCT/MCTES for an Assistant Researcher Position (ref. CEECIND/02128/2017) funded through the Individual Call to Scientific Employment Stimulus (https://doi.org/10.54499/CEECIND/02128/2017/CP1459/CT0039). The NMR spectrometers used in this work are part of the National NMR Network (PTNMR) and are partially supported by Infrastructure Project No. 022161 (POCI-01-0145-FEDER-022161, co-financed by FEDER through COMPETE 2020, POCI and PORL, and FCT through PIDDAC).

References

1 M. E. Bowden and D. A. Casteel, *Bull. Hist. Chem.*, 2019, **44**, 10–17.
2 W. M. Cruickshank, *J. Nat. Philos. Chem. Arts*, 1801, **5**, 201–211.
3 C. P. Hopper, P. N. Zambrana, U. Goebel and J. Wollborn, *Nitric Oxide*, 2021, **111–112**, 45–63, DOI: **10.1016/j.niox.2021.04.001**.
4 H. P. Kim, S. W. Ryter and A. M. K. Choi, *Annu. Rev. Pharmacol. Toxicol.*, 2006, **46**, 411–449, DOI: **10.1146/annurev.pharmtox.46.120604.141053**.
5 R. Motterlini and L. E. Otterbein, *Nat. Rev. Drug Discovery*, 2010, **9**, 728–743, DOI: **10.1038/nrd3228**.
6 K. Ling, F. Men, W.-C. Wang, Y.-Q. Zhou, H.-W. Zhang and D.-W. Ye, *J. Med. Chem.*, 2018, **61**, 2611–2635, DOI: **10.1021/acs.jmedchem.6b01153**.
7 R. Siracusa, A. Schaufler, V. Calabrese, P. M. Fuller and L. E. Otterbein, *Trends Pharmacol. Sci.*, 2021, **42**, 329–339, DOI: **10.1016/j.tips.2021.02.003**.
8 U. Goebel and J. Wollborn, *ICMx*, 2020, **8**, 2, DOI: **10.1186/s40635-020-0292-8**.
9 X. Ji, K. Damera, Y. Zheng, B. Yu, L. E. Otterbein and B. Wang, *J. Pharm. Sci.*, 2016, **105**, 406–416, DOI: **10.1016/j.xphs.2015.10.018**.
10 C. C. Romão, W. A. Blätter, J. D. Seixas and G. J. L. Bernardes, *Chem. Soc. Rev.*, 2012, **41**, 3571–3583, DOI: **10.1039/C2CS15317C**.
11 S. García-Gallego and G. J. L. Bernardes, *Angew. Chem., Int. Ed.*, 2014, **53**, 9712–9721, DOI: **10.1002/anie.201311225**.
12 H.-I. Choi, A. Zeb, M.-S. Kim, I. Rana, N. Khan, O. S. Qureshi, C.-W. Lim, J.-S. Park, Z. Gao, H.-J. Maeng and J.-K. Kim, *J. Controlled Release*, 2022, **350**, 652–667, DOI: **10.1016/j.jconrel.2022.08.055**.
13 R. Motterlini, J. E. Clark, R. Foresti, P. Sarathchandra, B. E. Mann and C. J. Green, *Circ. Res.*, 2002, **90**, e17–e24, DOI: **10.1161/hh0202.104530**.
14 J. E. Clark, P. Naughton, S. Shurey, C. J. Green, T. R. Johnson, B. E. Mann, R. Foresti and R. Motterlini, *Circ. Res.*, 2003, **93**, e2–e8, DOI: **10.1161/01.RES.0000084381.86567.08**.
15 T. R. Johnson, B. E. Mann, J. E. Clark, R. Foresti, C. J. Green and R. Motterlini, *Angew. Chem., Int. Ed.*, 2003, **42**, 3722–3729, DOI: **10.1002/anie.200301634**.
16 J. G. McKendrick and W. Snodgrass, *Br. Med. J.*, 1891, **1**, 1215, DOI: **10.1136/bmj.1.1588.1215**.
17 J. G. McKendrick and W. Snodgrass, *Nature*, 1891, **44**, 70–71, DOI: **10.1038/044070b0**.
18 A. Jurowska, K. Jurowski, J. Szklarzewicz, B. Buszewski, T. Kalenik and W. Piekoszewski, *Curr. Med. Chem.*, 2016, **23**, 3322–3342, DOI: **10.2174/0929867323666160504103743**.
19 M. J. Romão, *Dalton Trans.*, 2009, 4053–4068, DOI: **10.1039/B821108F**.
20 J. D. Seixas, A. Mukhopadhyay, T. Santos-Silva, L. E. Otterbein, D. J. Gallo, S. S. Rodrigues, B. H. Guerreiro, A. M. L. Gonçalves, N. Penacho, A. R. Marques, A. C. Coelho, P. M. Reis, M. J. Romão and C. C. Romão, *Dalton Trans.*, 2013, **42**, 5985–5998, DOI: **10.1039/c2dt32174b**.
21 P. Köpf-Maier, M. Leitner, R. Voigtländer and H. Köpf, *Z. Naturforsch. C*, 1979, **34**, 1174–1176, DOI: **10.1515/znc-1979-1215**.
22 E. Meléndez, *J. Organomet. Chem.*, 2012, **706–707**, 4–12, DOI: **10.1016/j.jorganchem.2012.02.006**.
23 P. M. Abeysinghe and M. M. Harding, *Dalton Trans.*, 2007, 3474–3482, DOI: **10.1039/B707440A**.
24 J. B. Waern and M. M. Harding, *J. Organomet. Chem.*, 2004, **689**, 4655–4668, DOI: **10.1016/j.jorganchem.2004.08.014**.
25 Y.-X. Wang, P. Legzdins, J. S. Poon and C. C. Y. Pang, *J. Cardiovasc. Pharmacol.*, 2000, **35**, 73–77, DOI: **10.1097/00005344-200001000-00009**.
26 B. El Mouatassim, H. ElAmouri, M. Salmain and G. Jaouen, *J. Organomet. Chem.*, 1994, **479**, c18–c20, DOI: **10.1016/0022-328X(94)84121-7**.
27 M. R. P. Norton Matos, C. C. Romão, C. C. L. Pereira, S. S. Rodrigues, M. Mora, M. J. P. Silva, P. M. Alves and C. A. Reis, *Int. Pat.* WO/2005/087783, 2005.
28 C. C. L. Pereira, C. V. Diogo, A. Burgeiro, P. J. Oliveira, M. P. M. Marques, S. S. Braga, F. A. A. Paz, M. Pillinger and I. S. Gonçalves, *Organometallics*, 2008, **27**, 4948–4956, DOI: **10.1021/om800413w**.
29 S. S. Braga, V. Mokal, F. A. A. Paz, M. Pillinger, A. F. Branco, V. A. Sardão, C. V. Diogo, P. J. Oliveira, M. P. M. Marques, C. C. Romão and I. S. Gonçalves, *Eur. J. Inorg. Chem.*, 2014, 5034–5045, DOI: **10.1002/ejic.201402540**.
30 I. Honzíčková, J. Vinklárek, Z. Růžičková, M. Řezáčová and J. Honzíček, *Appl. Organomet. Chem.*, 2017, **31**, e3759, DOI: **10.1002/aoc.3759**.
31 O. Mrózek, L. Šebestová, J. Vinklárek, M. Řezáčová, A. Eisner, Z. Růžičková and J. Honzíček, *Eur. J. Inorg. Chem.*, 2016, 519–529, DOI: **10.1002/ejic.201501133**.
32 I. J. S. Fairlamb, J. M. Lynam, B. E. Moulton, I. E. Taylor, A.-K. Duhme-Klair, P. Sawle and R. Motterlini, *Dalton Trans.*, 2007, 3603–3605, DOI: **10.1039/B707377A**.
33 W.-Q. Zhang, A. J. Atkin, I. J. S. Fairlamb, A. C. Whitwood and J. M. Lynam, *Organometallics*, 2011, **30**, 4643–4654, DOI: **10.1021/om200495h**.
34 A. Kubicka, E. Parfieniuk, E. Fornal, M. Palusiak, D. Lizińska, A. Gumieniczek and B. Rudolf, *J. Photochem. Photobiol., A*, 2018, **351**, 115–123, DOI: **10.1016/j.jphotochem.2017.10.012**.

35 A. F. N. Tavares, M. Teixeira, C. C. Romão, J. D. Seixas, L. S. Nobre and L. M. Saraiva, *J. Biol. Chem.*, 2011, **286**, 26708–26717, DOI: **10.1074/jbc.M111.255752**.
36 L. S. Nobre, H. Jeremias, C. C. Romão and L. M. Saraiva, *Dalton Trans.*, 2016, **45**, 1455–1466, DOI: **10.1039/c5dt02238j**.
37 W.-Q. Zhang, A. J. Atkin, R. J. Thatcher, A. C. Whitwood, I. J. S. Fairlamb and J. M. Lynam, *Dalton Trans.*, 2009, 4351–4358, DOI: **10.1039/B822157J**.
38 W. Q. Zhang, A. C. Whitwood, I. J. S. Fairlamb and J. M. Lynam, *Inorg. Chem.*, 2010, **49**, 8941–8952, DOI: **10.1021/ic101230j**.
39 P. Wang, H. Liu, Q. Zhao, Y. Chen, B. Liu, B. Zhang and Q. Zheng, *Eur. J. Med. Chem.*, 2014, **74**, 199–215, DOI: **10.1016/j.ejmech.2013.12.041**.
40 H. Liu, P. Wang, Q. Zhao, Y. Chen, B. Liu, B. Zhang and Q. Zheng, *Appl. Organomet. Chem.*, 2014, **28**, 169–179, DOI: **10.1002/aoc.3105**.
41 L. Kromer, A. C. Coelho, I. Bento, A. R. Marques and C. C. Romão, *J. Organomet. Chem.*, 2014, **760**, 89–100, DOI: **10.1016/j.jorganchem.2013.12.009**.
42 H. Pfeiffer, T. Sowik and U. Schatzschneider, *J. Organomet. Chem.*, 2013, **734**, 17–24, DOI: **10.1016/j.jorganchem.2012.09.016**.
43 E. Parera, M. Marín-García, R. Pons, F. Comelles, J. Suades and R. Barnadas-Rodríguez, *Organometallics*, 2016, **35**, 484–493, DOI: **10.1021/acs.organomet.5b00917**.
44 A. R. Marques, L. Kromer, D. J. Gallo, N. Penacho, S. S. Rodrigues, J. D. Seixas, G. J. L. Bernardes, P. M. Reis, S. L. Otterbein, R. A. Ruggieri, A. S. G. Gonçalves, A. M. L. Gonçalves, M. N. de Matos, I. Bento, L. E. Otterbein, W. A. Blättler and C. C. Romão, *Organometallics*, 2012, **31**, 5810–5822, DOI: **10.1021/om300360c**.
45 N. Schallner, C. C. Romão, J. Biermann, W. A. Lagrèze, L. E. Otterbein, H. Buerkle, T. Loop and U. Goebel, *PLoS One*, 2013, **8**, e60672, DOI: **10.1371/journal.pone.0060672**.
46 S. X. Lee, C. H. Tan, W. L. Mah, R. C. S. Wong, Y. L. Cheow, K. S. Sim and K. W. Tan, *Inorg. Chim. Acta*, 2021, **524**, 120491, DOI: **10.1016/j.ica.2021.120491**.
47 S. X. Lee, C. H. Tan, W. L. Mah, R. C. S. Wong, N. S. A. Manan, Y. L. Cheow, K. S. Sim and K. W. Tan, *Inorg. Chim. Acta*, 2022, **537**, 120931, DOI: **10.1016/j.ica.2022.120931**.
48 H. Inaba, K. Fujita and T. Ueno, *Biomater. Sci.*, 2015, **3**, 1423–1438, DOI: **10.1039/C5BM00210A**.
49 A. C. Kautz, P. C. Kunz and C. Janiak, *Dalton Trans.*, 2016, **45**, 18045–18063, DOI: **10.1039/c6dt03515a**.
50 A. Carné-Sánchez, F. J. Carmona, C. Kim and S. Furukawa, *Chem. Commun.*, 2020, **56**, 9750–9766, DOI: **10.1039/D0CC03740K**.
51 F. J. Carmona, S. Rojas, C. C. Romão, J. A. R. Navarro, E. Barea and C. R. Maldonado, *Chem. Commun.*, 2017, **53**, 6581–6584, DOI: **10.1039/c7cc03605a**.
52 F. J. Carmona, C. R. Maldonado, S. Ikemura, C. C. Romão, Z. Huang, H. Xu, X. Zou, S. Kitagawa, S. Furukawa and E. Barea, *ACS Appl. Mater. Interfaces*, 2018, **10**, 31158–31167, DOI: **10.1021/acsami.8b11758**.
53 I. B. Calhau, A. C. Gomes, S. M. Bruno, A. C. Coelho, C. I. R. Magalhães, C. C. Romão, A. A. Valente, I. S. Gonçalves and M. Pillinger, *Eur. J. Inorg. Chem.*, 2020, 2726–2736, DOI: **10.1002/ejic.202000202**.
54 A. F. Silva, I. B. Calhau, A. C. Gomes, A. A. Valente, I. S. Gonçalves and M. Pillinger, *Mater. Sci. Eng., C*, 2021, **124**, 112053, DOI: **10.1016/j.msec.2021.112053**.
55 S. S. Braga, F. A. A. Paz, M. Pillinger, J. D. Seixas, C. C. Romão and I. S. Gonçalves, *Eur. J. Inorg. Chem.*, 2006, 1662–1669, DOI: **10.1002/ejic.200501006**.
56 S. S. Balula, A. C. Coelho, S. S. Braga, A. Hazell, A. A. Valente, M. Pillinger, J. D. Seixas, C. C. Romão and I. S. Gonçalves, *Organometallics*, 2007, **26**, 6857–6863, DOI: **10.1021/om701025z**.
57 P. Jansook, N. Ogawa and T. Loftsson, *Int. J. Pharm.*, 2018, **535**, 272–284, DOI: **10.1016/j.ijpharm.2017.11.018**.
58 J. Wankar, N. G. Kotla, S. Gera, S. Rasala, A. Pandit and Y. A. Rochev, *Adv. Funct. Mater.*, 2020, **30**, 1909049, DOI: **10.1002/adfm.201909049**.
59 D. Das, K. I. Assaf and W. M. Nau, *Front. Chem.*, 2019, **7**, 619, DOI: **10.3389/fchem.2019.00619**.
60 D. P. Buck, P. M. Abeysinghe, C. Cullinan, A. I. Day, J. G. Collins and M. M. Harding, *Dalton Trans.*, 2008, 2328–2334, DOI: **10.1039/B718322D**.
61 P. Neves, A. C. Gomes, R. P. Monteiro, M. J. Santos, A. A. Valente, A. D. Lopes, I. S. Gonçalves and M. Pillinger, *Appl. Organomet. Chem.*, 2024, **38**, e7412, DOI: **10.1002/aoc.7412**.
62 A. C. Gomes, R. P. Monteiro, I. B. Calhau, A. D. Lopes, I. S. Gonçalves and M. Pillinger, *J. Organomet. Chem.*, 2024, **1019**, 123312, DOI: **10.1016/j.jorganchem.2024.123312**.
63 T. S. Piper and G. Wilkinson, *J. Inorg. Nucl. Chem.*, 1956, **3**, 104–124, DOI: **10.1016/0022-1902(56)80073-0**.
64 R. King, *Organometallic Synthesis*, Academic Press, New York, 1965, vol. 1.
65 A. C. Gomes, C. I. R. Magalhães, T. S. M. Oliveira, A. D. Lopes, I. S. Gonçalves and M. Pillinger, *Dalton Trans.*, 2016, **45**, 17042–17052, DOI: **10.1039/c6dt02811j**.
66 A. J. Atkin, J. M. Lynam, B. E. Moulton, P. Sawle, R. Motterlini, N. M. Boyle, M. T. Pryce and I. J. S. Fairlamb, *Dalton Trans.*, 2011, **40**, 5755–5761, DOI: **10.1039/C0DT01809K**.
67 E. Antonini, *Physiol. Rev.*, 1965, **45**, 123–170, DOI: **10.1152/physrev.1965.45.1.123**.
68 S. S. Braga, I. S. Gonçalves, A. D. Lopes, M. Pillinger, J. Rocha, C. C. Romão and J. J. C. Teixeira-Dias, *Dalton Trans.*, 2000, 2964–2968, DOI: **10.1039/b003763j**.
69 S. Lima, I. S. Gonçalves, P. Ribeiro-Claro, M. Pillinger, A. D. Lopes, P. Ferreira, J. J. C. Teixeira-Dias, J. Rocha and C. C. Romão, *Organometallics*, 2001, **20**, 2191–2197, DOI: **10.1021/om001088s**.
70 R. Kumar, A. K. Thakur, N. Banerjee, A. Kumar, G. K. Gaurav and R. K. Arya, *Drug Delivery Transl. Res.*, 2023, **13**, 400–418, DOI: **10.1007/s13346-022-01219-1**.

71 M. Vogt, K. Kunath and J. B. Dressman, *Eur. J. Pharm. Biopharm.*, 2008, **68**, 330–337, DOI: **10.1016/j.ejpb.2007.05.009**.
72 M. Jug and P. A. Mura, *Pharmaceutics*, 2018, **10**, 189, DOI: **10.3390/pharmaceutics10040189**.
73 M. R. Caira, *Rev. Roum. Chim.*, 2001, **46**, 371–386.
74 V. J. Smith, N. M. Rougier, R. H. de Rossi, M. R. Caira, E. I. Buján, M. A. Fernández and S. A. Bourne, *Carbohydr. Res.*, 2009, **344**, 2388–2393, DOI: **10.1016/j.carres.2009.08.036**.
75 A. C. Gomes, C. I. R. Magalhães, T. S. M. Oliveira, A. D. Lopes, I. S. Gonçalves and M. Pillinger, *Dalton Trans.*, 2016, **45**, 17042–17052, DOI: **10.1039/c6dt02811j**.
76 M. J. Calhorda, *Chem. Commun.*, 2000, 801–809, DOI: **10.1039/A900221I**.
77 S. J. Heyes, N. J. Clayden and C. M. Dobson, *Carbohydr. Res.*, 1992, **233**, 1–14, DOI: **10.1016/S0008-6215(00)90916-9**.
78 N. Grover, A. Pöthig and F. E. Kühn, *Catal. Sci. Technol.*, 2014, **4**, 4219–4231, DOI: **10.1039/c4cy00738g**.
79 M. Abrantes, P. Neves, M. M. Antunes, S. Gago, F. A. A. Paz, A. E. Rodrigues, M. Pillinger, I. S. Gonçalves, C. M. Silva and A. A. Valente, *J. Mol. Catal. A: Chem.*, 2010, **320**, 19–26, DOI: **10.1016/j.molcata.2009.12.011**.
80 P. S. Bruni and S. Schürch, *Int. J. Mol. Sci.*, 2021, **22**, 9789, DOI: **10.3390/ijms22189789**.
81 R. Bakhtiar and A. E. Kaifer, *Rapid Commun. Mass Spectrom.*, 1998, **12**, 111–114, DOI: **10.1002/(SICI)1097-0231(19980214)12:3%3C111::AID-RCM135%3E3.0.CO;2-D**.
82 I. Turel, A. Demšar and J. Košmrlj, *J. Inclusion Phenom. Macrocyclic Chem.*, 1999, **35**, 595–604, DOI: **10.1023/A:1008026715964**.
83 V. Iglesias, M. R. Avei, S. Bruña, I. Cuadrado and A. E. Kaifer, *J. Org. Chem.*, 2017, **82**, 415–419, DOI: **10.1021/acs.joc.6b02508**.
84 J. P. Da Silva, N. Jayaraj, S. Jockusch, N. J. Turro and V. Ramamurthy, *Org. Lett.*, 2011, **13**, 2410–2413, DOI: **10.1021/ol200647j**.
85 H. G. Alt and J. A. Schwärzle, *J. Organomet. Chem.*, 1978, **162**, 45–56, DOI: **10.1016/S0022-328X(00)89079-8**.
86 S. McLean, B. E. Mann and R. K. Poole, *Anal. Biochem.*, 2012, **427**, 36–40, DOI: **10.1016/j.ab.2012.04.026**.
87 H. M. Southam, M. P. Williamson, J. A. Chapman, R. L. Lyon, C. R. Trevitt, P. J. F. Henderson and R. K. Poole, *Antioxidants*, 2021, **10**, 915, DOI: **10.3390/antiox10060915**.